Parallel Fully-Implicit Computation of Magnetohydrodynamics Acceleration Experiments

Tian Wan[a, *] and Graham Candler[b]

[a]*Assistant professor. LHD, Institute of Mechanics, Chinese Academy of Sciences*
*(*wtsmile@126.com)*
[b]*Professor. Aerospace Engineering and Mechanics Department, University of Minnesota*

Abstract. A three-dimensional MHD solver is described in the paper. The solver simulates reacting flows with nonequilibrium between translational-rotational, vibrational and electron translational modes. The conservation equations are discretized with implicit time marching and the second-order modified Steger-Warming scheme, and the resulted linear system is solved iteratively with Newton-Krylov-Schwarz method that is implemented by PETSc package. The results of convergence tests are plotted, which show good scalability and convergence around twice faster when compared with the DPLR method. Then five test runs are conducted simulating the experiments done at the NASA Ames MHD channel, and the calculated pressures, temperatures, electrical conductivity, back EMF, load factors and flow accelerations are shown to agree with the experimental data. Our computation shows that the electrical conductivity distribution is not uniform in the powered section of the MHD channel, and that it is important to include Joule heating in order to calculate the correct conductivity and the MHD acceleration.

Keywords: Electron-temperature, Joule heating, fully-implicit method.
PACS: 47.65.-d

INTRODUCTION

Magnetohydrodynamics (MHD) can be utilized to increase the performance of propulsion systems as it can accelerate flows significantly within a relatively short distance. Moreover, MHD modifies flows through electromagnetic forces, which makes it work at conditions beyond those of traditional propulsion methods. In order to study MHD acceleration, experimental data were obtained at the MHD channel at NASA Ames Research Center by Bogdanoff, Park and Mehta.[1] A total of fourteen test runs were reported in the experimental paper, where the flow quantities and electrical parameters were measured and presented. The results showed that up to 40% acceleration was achieved in an approximately half-meter long channel, where around half of the channel was powered by 17 pairs of electrodes. The channel operated at atmospheric pressure with flow Mach number around two and temperature 3000 - 4000 K. 1% potassium by mass of the driven gas was injected into the driven tube before entering the nozzle. The averaged magnetic field in the channel was about 0.92T.

The experiments were simulated by Gupta and Tannehill[2] from Iowa State University. In their work, Parabolized Navier-Stokes (PNS) equations were solved, and three different chemistry models were used: perfect gas, equilibrium and nonequilibrium air-seed chemistry. The vibrational and electron translational nonequilibrium were not considered, and the electrical conductivity was assumed constant in their work. Their computed pressure showed good agreement with the experimentally measured data. However, for run 15 and 20, their computation underestimated the velocity at the channel exit when the measured value of electric field was used. In our present work, we simulate the same experiments by solving chemically reacting, three-dimensional Navier-Stokes equations including the vibrational and electron energy conservation equation. We will show that the electrical conductivity increases in the streamwise direction due to Joule heating of electrons. Assuming low magnetic Reynolds number, we model MHD effects as source terms in the conservation equations. Implicit time marching and the modified second-order Steger-Warming[3] scheme are used to discretize the conservation equations, and the resulted linear

CP1233 *The 2nd International ISCM Symposium and The 12th International EPMESC Conference*
J. W. Z. Lu, A.Y.T. Leung, V. P. Iu, and K. M. Mok

system is solved iteratively by Newton-Krylov-Schwarz method. In the following sections, the governing equations of the MHD solver are given, together with descriptions of the models for energy exchange mechanisms and electron transport coefficients. The principles of the numerical method are introduced, followed by convergence and scalability tests on a grid of half-million points. Then the MHD acceleration experiments are simulated, and the results of five test runs are shown and compared with the measured data. From the computed data, we plot the pressure, temperature, conductivity, and back EMF to test the models that are currently in the MHD solver. The flow accelerations and load factors at different MHD power levels are also calculated. The conclusions and future research directions are given in the last section.

GOVERNING EQUATIONS OF THE MHD FLOW SOLVER

We use a five-species (N_2, O_2, NO, N, O) air chemistry model.[3] Including the seed species (potassium atom and ion, electron), a total of eight equations are solved for mass conservation, which take the form

$$\frac{\partial \rho_s}{\partial t} + \nabla \cdot (\rho_s \vec{u}) + \nabla \cdot (\rho_s \vec{v}_s) = \omega_s. \tag{1}$$

Please refer to our previous work[4] for the details of the diffusion model. The momentum equation has an additional term and is expressed as

$$\frac{\partial (\rho \vec{u})}{\partial t} + \nabla \cdot (\rho \vec{u} \otimes \vec{u}) + \nabla p + \nabla \cdot \tau = \vec{j} \times \vec{B}, \tag{2}$$

where the Lorentz force appears on the right hand side.

The conservation equations for vibrational energy and electron energy are given by

$$\frac{\partial E_v}{\partial t} + \nabla \cdot (E_v \vec{u}) = -\nabla \cdot \sum_{s=1}^{ns} \vec{v}_s E_{v,s} - \nabla \cdot \vec{q}_v + Q_{T-v} + Q_{e-v} + \sum_{s=1}^{ns} \omega_s e_{v,s}, \tag{3}$$

$$\frac{\partial E_e}{\partial t} + \nabla \cdot ((E_e + p_e)(\vec{u} + \vec{v}_e)) = -\nabla \cdot \vec{q}_e - Q_{h-e} - Q_{e-v} + (\vec{j} \cdot \vec{j})/\sigma_e + \omega_e e_e, \tag{4}$$

where E_v and E_e are the vibrational and electron energy terms, $e_{v,s}$ is the specific vibrational energy for species s and p_e is the electron partial pressure. Q_{T-v} and Q_{e-v} are respectively the rates of translational-vibrational and electron-vibrational energy exchange, and Q_{h-e} represents the rate of energy exchange between heavy particles and electrons. $\sum_{s=1}^{ns} \omega_s e_{v,s}$ and $\omega_e e_e$ are source terms due to chemical reactions. The term $(\vec{j} \cdot \vec{j})/\sigma_e$ in the electron energy equation stands for energy addition by Joule heating.

The energy exchange rate between translational and vibrational modes can be found in [3]. The electron-translational and electron-vibrational energy exchange rates are given respectively by:

$$Q_{h-e} = n_e \sum_h 3k(T_e - T)(m_e / m_h)\delta_{eh} \nu_{eh}, \tag{5}$$

$$Q_{v-e} = \frac{E^*_{vN_2}(T_e) - E_{vN_2}}{\tau_{ve}}, \tag{6}$$

where ν_{eh} is the average collision frequency of the electrons with heavy particles.[4] The coupling of the electron energy with the vibrational energy is much stronger for N_2 compared to the other species of air,[5] hence the contribution of other species to electron-vibrational relaxation is neglected. The nonelastic energy factor δ_{eh} is set to a value of 1000.[6] The relaxation time τ_{ve} can be found in [7].

The equation for conservation of the total energy is given by

$$\frac{\partial E}{\partial t} + \nabla \cdot ((E + p)\vec{u}) = -\nabla \cdot (\vec{q} + \vec{q}_v + \vec{q}_e) - \nabla \cdot (\vec{u} \cdot \vec{\tau}) - \nabla \cdot \sum_{s=1}^{ns} (\vec{v}_s \rho_s h_s) + \vec{j} \cdot \vec{E}, \tag{7}$$

where the last term on the right hand side is the MHD power input, and the electron heat conduction vector $\vec{q}_e$ is given by

$$\vec{q}_e = -\kappa_e \nabla T_e, \tag{8}$$

where κ_e is the electron thermal conductivity

$$\kappa_e = \frac{2.4k^2 n_e T_e}{m_e \nu_{eh}}. \tag{9}$$

In the scope of present work, Hall effect and Ion slip are negligible, and the electric current density $\vec{j}$ is computed from Ohm's law

$$\vec{j} = \sigma_e(\vec{E} + \vec{u} \times \vec{B}). \tag{10}$$

For electrical conductivity σ_e we use the Frost formula[8]

$$\sigma_e = \frac{4\pi n_e e^2}{3kT_e} \int_0^\infty \frac{C^4 f_M}{\nu_{eh}} dC, \tag{11}$$

where f_M is the Maxwellian velocity distribution function. The one-equation Spalart-Allmaras RANS turbulence model is used in the current work.

NUMERICAL METHOD

The conservation equations are discretized with the modified second-order Steger-Warming scheme.[3] After discretization, the system has the form

$$\frac{d\mathbf{U}}{dt} = -\frac{1}{V_{i,j,k}}\mathbf{R}, \tag{12}$$

where $\mathbf{U}$ is the vector of unknown variables and $\mathbf{R}$ is the residual. Then the implicit Euler time-marching is applied

$$\left[\frac{\mathbf{I}}{\Delta t} + \mathbf{A}\right]^{(n)} \Delta\mathbf{U}^{(n)} = -\mathbf{R}^{(n)}, \tag{13}$$

where $\mathbf{A}$ is the summation of the flow Jacobians and Δt is the time step. Equation (13) is referred as Inexact-Newton method due to the additional time step term. If $\Delta t \to 0$, Newton's method is recovered.

Directly solving the large sparse linear system resulted from equation (13) is prohibitively expensive, therefore simplification of the implicit part of the system is needed to reduce the cost. For example, DPLUR and DPLR[9] methods move certain implicit terms to the right hand side so that efficient direct solvers can be applied. Newton-Krylov methods take a different approach by transforming the system with preconditioners

$$\mathbf{P}^{-1}\left[\frac{\mathbf{I}}{\Delta t} + \mathbf{A}\right]^{(n)} \Delta\mathbf{U}^{(n)} = -\mathbf{P}^{-1}\mathbf{R}^{(n)}. \tag{14}$$

The effect of the preconditioner, $\mathbf{P}$ in the above equation, is rescaling the eigenvalue spectrum of the system to near unity. In the present paper, we use the Newton-Krylov-Schwarz method from [10] and implement it by including PETSc package.[11] Namely, domain decomposition is applied for parallelization, and we use an ILU(0) preconditioner and the GMRES method in every sub-domain, together with the restricted additive Schwarz method for inter-domain convergence acceleration.

NUMERICAL RESULTS

The experimental data were obtained at the MHD channel at NASA Ames Research Center by Bogdanoff, Park and Mehta.[1] The simulations were performed on a grid of 251×51×51 points with minimum near-wall spacing 10^{-6}, and because of the flow symmetry, only a quarter of the nozzle and channel cross section was computed. The averaged magnetic field in the channel was about 0.92 Tesla.

As the initial conditions for the simulations, zero velocity and high pressure and temperature were set at the nozzle entrance. Temperature at the channel wall and electrodes was assumed constant as 300 K, while for electron temperature zero-gradient boundary condition was applied. We simulated five experimental runs. The nozzle entrance conditions and computed electric field strength for these five runs are listed in Table 1. The electric field strengths were determined by taking the measured voltage drop across the central flow and dividing by the channel height. The electrodes were open-circuited in the experiments when MHD power was off; hence for Run 9 we determined the electric field by assigning a load factor of negative one. The streamwise component of electric field and the Hall effect were neglected as the MHD channel operates in the segmented Faraday mode. The voltage drop in the boundary layer and sheath is neglected in the scope of the present paper.

TABLE 1. Flow parameters for the five simulation runs.

Case	Nozzle entrance pressure (atm)	Nozzle entrance temperature (K)	Capacitor voltage (V)	Electric field (V/m)
Run 9	8.3	5560	0	Load factor = -1
Run 13	9.9	5560	210	3400
Run 15	8.4	5560	320	4130
Run 20	10.6	5560	380	4500
Run noB	9.9	5560	260	3540

Parallel scalability, speedup and memory usage were tested on a cluster of dual-processor, dual-core, 2.2 GHz, AMD Opteron, 64-bit computers with 4 GBytes of memory per computer node. The Portland Group compilers and OpenMPI were used for producing the executables, including the PETSc library. Fig. 1 plots the convergence history for the channel flow computation with the same series of CFL numbers used, which shows that the fully coupled method converges twice as fast as DPLR. The reason for this difference is that DPLR only performs implicit relaxation in one direction, while the fully coupled method does unbiased global implicit relaxation in every subdomain.

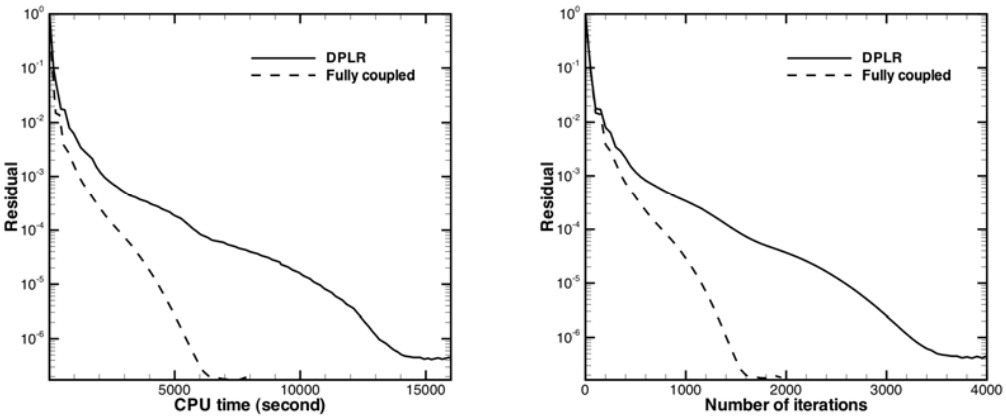

(a) CPU time (b) Iteration

FIGURE 1. Convergence rates of the fully coupled and DPLR method.

Figure 2 plots the pressure distribution along the channel centerline for run 13, 15 and 20. They show that the computed pressure agrees with the experimentally measured value. Figure 3 plots the translational, vibrational and electron temperature, as well as the conductivity distribution along the channel centerline. The figure shows that the electron temperature nonequilibrium is not significant due to the high pressure in the channel. The Joule heating, one the other hand is very important and hence solving the electron temperature equation is necessary. The nonelastic factor in the energy exchange rate between translational and electron energy mode is set to be 1000. The peak temperature in the channel becomes larger as the power input increases, as a result of Joule heating and energy exchange between electrons and heavy particles. The computed conductivity based on electron temperature is compared with measured data, and they are in good agreement.

Gupta and Tannehill using a PNS and equilibrium model simulated the experiments. In their results, the computed velocity of run 20 was underpredicted compared to the experimental data. In the present work, computations are conducted with both electron temperature equilibrium and nonequilibrium model. With the nonequilibrium model, the electron energy equation is solved and the conductivity is computed based on the electron temperature; whereas with the equilibrium model, the electron energy conservation equation was not solved, instead, the electron temperature is forced equal to the translational temperature, and the conductivity is computed using the translational temperature. The computed results for run 20 are shown in Fig. 4. The equilibrium conductivity is lower than the nonequilibrium one, because it is unable to predict the Joule heating with the equilibrium model. The lower conductivity causes smaller flow acceleration as shown in the figure.

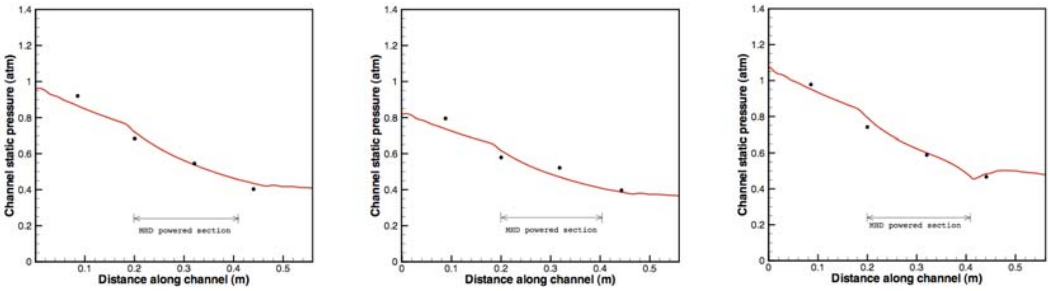

(a) Run 13 (b) Run 15 (c) Run 20

FIGURE 2. Static pressure of runs 13, 15 and 20 along the channel centerline. The dots are the measured data, and the lines are the computational results.

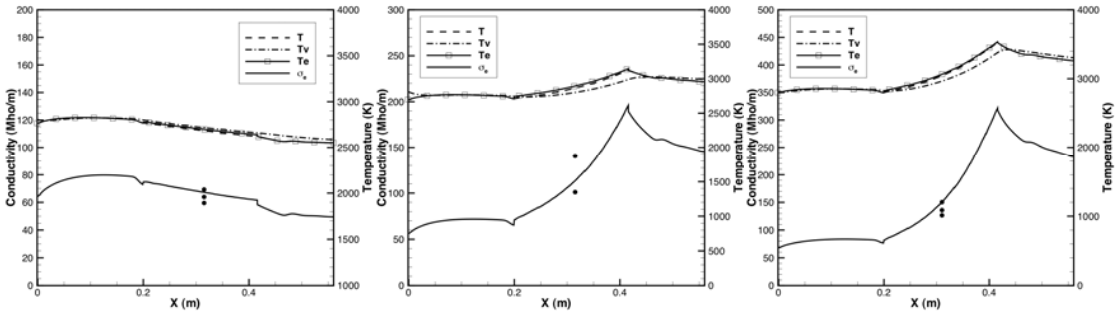

(a) Run 13 (b) Run 15 (c) Run 20

FIGURE 3. Translational, vibrational and electron temperature, and conductivity of runs 13, 15 and 20 along the channel centerline. The dots are the measured data, and the lines are the computational results.

The computed flow acceleration is plotted in Fig. 4, all using the nonequilibrium model. The velocity is first averaged across the channel cross section at the location of electrode pair 19, then it is normalized by the velocity with magnetic field on and MHD power off. It shows that the computed acceleration agrees with the experimental value. After comparison with the results of Gupta and Tannehill, it is concluded that modeling the Joule heating is essential.

CONCLUSIONS

A three-dimensional MHD flow solver was described in the present paper. The solver can simulate viscous reacting flows, with relaxation between translation-rotational, vibrational and electron-translational modes included. The effects of MHD on flows, namely Lorentz force, Joule heating and MHD power input, were incorporated as source terms. The models of electrical conductivity, electron thermal conductivity and collision frequencies were taken from the corresponding references. The conservation equations were discretized with the second-order modified Steger-Warming scheme, and the Inexact-Newton method was used to linearize the discretized equations, which were then solved iteratively by the GMRES method. Parallelization was realized by domain decomposition, and the Schwarz method was applied to achieve inter-domain convergence acceleration. The fully coupled method was implemented by PETSc routines. Good scalability and convergence rates were achieved by the fully coupled method, and when compared with the DPLR method, the fully coupled method converges about twice faster in terms of CPU time.

The experiments conducted at the MHD channel at NASA Ames Research Center by Bogdanoff, Park and Mehta were simulated. A total of five runs were computed. Three runs were with both magnetic field and MHD power on; one was with magnetic field but no MHD power; the last run was conducted with MHD power but no magnetic field. The computed channel static pressures agreed with the experiment data. The translational, vibrational and electron temperature were plotted for the three test runs with MHD power on, which showed insignificant nonequilibrium (about 200 K maximum). However, it was shown that Joule heating had large influence on the conductivity and solving the electron energy equation was necessary. With increasing MHD power level, the peak electron

temperature increased, and so did the translational and vibrational temperature due to energy exchange between electrons and heavy particles. Then computed nonequilibrium electrical conductivity was plotted, and the results agreed with the experiments. Run 20 was simulated with both electron temperature equilibrium and nonequilibrium model. The results showed that only the nonequilibrium simulations predict the correct MHD acceleration, whereas the equilibrium model underpredicted the conductivity and flow velocity. Conducted to measure the normalization velocity in the acceleration evaluation, the experiment run without MHD power was simulated. The MHD accelerations were plotted, and they agreed well with the experiments. In summary, our computational model and tool are accurate for the presented type of flow.

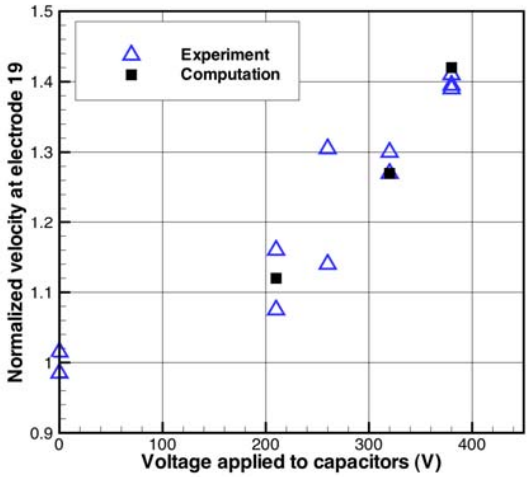

FIGURE 4. Normalized velocities at the last electrode pair at different MHD power levels. The velocities are averaged across the channel cross section.

REFERENCES

1. D. W. Bogdanoff, and U. B. Mehta, "Experimental Demonstration of Magneto-hydro-dynamic (MHD) Acceleration," AIAA Paper 2003-4285, June 2003.
2. S. Gupta, J. C. Tannehill, and U. B. Mehta, "Simulation of 3-D Nonequilibrium Seeded Air Flow in the NASA-Ames MHD Channel," *Journal of Thermophysics and Heat Transfer*, 2007, 0887-8722 vol.21 no.2 (276-283)
3. G. V. Candler, "The Computation of Weakly Ionized Hypersonic Flows in Thermochemical Nonequilibrium," Ph.D. Thesis, Stanford University.
4. T. Wan, G. V. Candler, S. Macheret and M. Shneider, "Three Dimensional Simulation of Electric Field and MHD Power Generation During Re-Entry," *AIAA Journal*, vol 47, No. 6, June 2009.
5. J. H. Lee, "Basic Governing Equations for the Flight Regime of Aeroassisted Orbital Transfer Vehicles," *Thermal Design of Aeroassisted Orbital Transfer Vehicles*, ed. H. F. Nelson, Progress in Aeronautics and Astronautics, Vol. 96.
6. C. O. Laux, L. Yu, D. M. Packan, R. J. Gessman, etc, "Ionization Mechanisms in Two-Temperature Air Plasmas," AIAA Paper 99-3476, June 1999.
7. J. H. Lee, "Electron-Impact Vibrational Relaxation in High-temperature Nitrogen," AIAA Paper 92-0807.
8. M. Mitchner and C. H. Kruger, *Partially Ionized Gases*, John Wiley & Sons, New York, 1973.
9. M. J. Wright, "A Family of Data-Parallel Relaxation Methods for the Navier-Stokes Equations," Ph.D. Thesis, University of Minnesota, 1997.
10. W. D. Gropp, D. K. Kaushik, D. E. Keyes, B. F. Smith, "High-performance Parallel Implicit CFD," *Parallel Computing*, 27, 337-362, 2001.
11. S. Balay, K. Buschelman, V. Eijkhout, W. D. Gropp, etc, "PETSc Users Manual," ANL-95/11-Revision 2.1.5, Argonne National Laboratory, 2004.